Macromolecules
ARTICLE

Macromolecules **2010**, *43*, 1041–1049 **1041**
DOI: 10.1021/ma9019448

Shear-Induced Nanometer and Micrometer Structural Responses in Nanocomposite Hydrogels

Elena Loizou,*,†,‡,§ Lionel Porcar,‡,∥,⊥ Patrick Schexnailder,# Gudrun Schmidt,# and Paul Butler‡

†*Louisiana State University, Baton Rouge, Louisiana 70803,* ‡*National Institute of Standards and Technology, Gaithersburg, Maryland 20899,* §*University of Cyprus, Nicosia, Cyprus,* ∥*University of Maryland, College Park, Maryland 20742,* ⊥*Institue Laue Langevin, Grenoble, France, and* #*Purdue University, West Lafayette, Indiana 47907*

Received September 1, 2009; Revised Manuscript Received December 3, 2009

ABSTRACT: The structural responses of a polymer−clay nanocomposite hydrogel to an imposed shear field are investigated from the nanometer to the micrometer length scales. The effects of polymer molecular weight and concentration of the components are probed, and the structural response of the individual components is explored using contrast matching techniques with small-angle neutron scattering. At rest the clay structure appears minimally perturbed by the presence of the polymer. As the network begins to be disrupted under the effect of low shear, large-scale inhomogeneities roll up and orient with their long axis parallel to the neutral direction. With increasing shear rates the effect of the polymer−clay interactions becomes apparent with nanoscopic orientation of both the clay platelets and the polymer chains, but only in systems where polymer bridging of the clay can occur. The clay and polymer concentration dependence of the shear response suggests an ideal combination of concentrations and polymer molecular weights with implications for materials design.

Introduction

Polymer and clay nanocomposite materials have attracted a considerable and growing interest over the past few decades. The novel physical properties of these materials have led to applications in such diverse areas as paints, coatings, cosmetics, pharmaceutical formulations, personal care products, and film barrier membranes.[1,2] The unique macroscopic and nanoscopic properties of these materials are derived from the physical presence of the clay nanoparticle, the interaction of the polymer with the clay nanoparticle, the state of dispersion of the clay nanoparticle, and the particle orientation within the polymer matrix. These macroscopic properties can thus be dramatically altered by tuning such parameters as composition, polymer molecular weight, flow fields, pH, and ionic strength, just to name a few.[3−12] A detailed understanding of the complex effects and interactions of these many factors is thus essential to the design of new materials suitable to a specific application and is the subject of many ongoing efforts. In this work, we use one of the most studied model systems for looking at polymer−clay structure and interactions and their responses to shear flow which consists of aqueous solutions of laponite clay nanoparticles dispersed in a poly(ethylene oxide) matrix.[5−21]

From the body of existing work it is clear that the PEO chains adsorb on the clay particles forming a layer that is roughly 1.5 nm thick on each face, independent of the polymer's molecular weight, at least in the range used in this work of 100−1000 kg/mol.[6,7,19] Low molecular weight polymers have been shown to hinder aggregation of clay particles through classic steric hindrance, either retarding or preventing the gelation process, and thus decrease the viscosity and elastic modulus of the dispersion.[6−9] Higher molecular weight polymers, especially at concentrations below the threshold for complete saturation of clay surface, produce "shake gels".[9−11] These gels are fluid but undergo a dramatic shear thickening behavior when subjected to vigorous shaking, in which state they can support their own weight upon inverting the vials. The shear-induced gelation is time reversible and strongly dependent on the PEO concentration and on temperature.[9] For concentrations of PEO in excess of that required for complete coverage, more permanent gels form in systems where the molecular weight is large enough to span the interplatelet distance (which depends on the clay concentration) and an associative network is formed, leading to an enhanced viscosity and elastic modulus. These gels have been reported to have a "chewing gum" consistency from which meter long fibers of micrometer diameter can be drawn.[14−16] More recently, it has also been noted that the addition of laponite to a concentrated polymer solution increases the relaxation time but decreases the elastic modulus of that system which is attributed to the polymer tethering clay particles.[22]

Upon subjecting these more permanent gels to a shear field, the network is stretched and the nanocomponents are forced to orient with, in this case, the clay platelets' face normal parallel to the neutral direction. It is suggested that the clay may align first followed by the stretching of polymer chain, at even higher shear rates.[14−16] Interestingly, a similar system using montmorillonite rather than laponite under shear shows the montmorillonite platelets aligning under shear in the more normal orientation with their face normal parallel to the shear gradient.[23] It remains unclear what drives this surprising difference.

Besides the alignment of the clay particles themselves, much larger, spatially modulated macrodomains have been shown to form in a very high molecular weight PEO system (of weight-average molecular weight M_w = 1000 kg/mol) under shear.[17,18] These large objects which orient with their long axis parallel to the neutral direction are thought to be due to both the clay and the network active PEO. Very recently, it has been suggested that the polymers tether the clay only above a certain critical shear rate.[5]

Despite this extensive body of research, much about these PEO−laponite systems remains poorly understood. Our recent interests have focused on the permanent gel region. Our overall

*Corresponding author. E-mail: elenaloizou@gmail.com.

Published on Web 12/22/2009

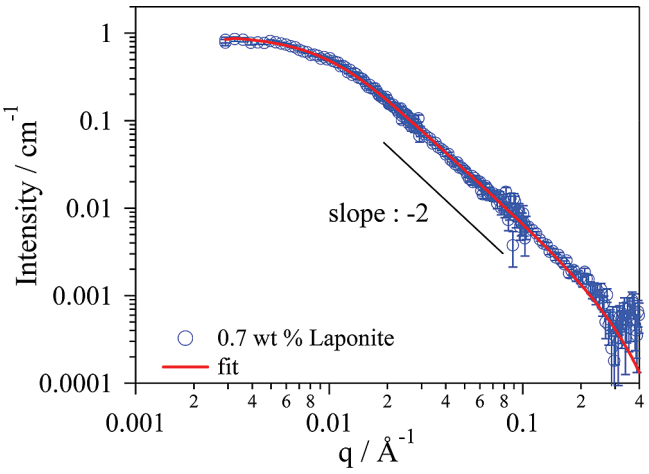

Figure 1. SANS data for a 0.7 wt % laponite dispersion in D_2O. The line is a fit to the data using a form factor for a disk with a polydisperse radius.

Table 1. Fit Parameters Derived from the Scattering of Laponite Dispersion in D_2O

parameters	0.7 wt % laponite
volume fraction	0.0029
particle radius (Å)	93.78 ± 3.52
particle height (Å)	9.01 ± 0.05
polydispersity of radius	0.56 ± 0.03
scattering length density difference (Å^{-2})	2.05×10^{-6}

objective however is to better understand the polymer−clay interactions in these hydrogels and how these interactions affect the nanoscopic and microscopic structures when subjected to shear flow. In the work presented here these structures were studied as a function of polymer molecular weight and polymer and clay concentrations. In particular, the response to shear flow of these changes and their implications for the mechanisms involved were examined. We also used contrast matching techniques available to neutron scattering to elucidate the contributions to the structures and structural changes that come from each of the individual components of the system (clay and polymer). We are thus able to begin to disentangle the contributions of each of the components as well as the effects of the polymer network from bridging effects.

Experimental Section

Laponite RD (LRD) was obtained from Southern Clay Products Inc. and used as received.[24] The clay particles are composed of platelets of high purity and relatively uniform size ≈20−30 nm in diameter and ≈1 nm thickness. The parameters for the batch of clay used in this work were determined by measuring the SANS (described below) from a dilute solution of 0.7 wt % laponite in D_2O with the charges screened and the pH adjusted as described below (Figure 1 and Table 1). The data can readily be fit by a disk model (note that a mass fraction of 0.007 in D_2O corresponds to a volume fraction of 0.003 given the density of laponite is 2.65 g cm^{-3}). Fixing both the volume fraction and scattering length density to the known values, an excellent fit is obtained with a plate thickness of 0.901 ± 0.005 nm, a radius of 9.4 ± 0.4 nm (diameter of 19 ± 1 nm), and a surprisingly strong (Shultz−Zimm) polydispersity of 0.56 ± 0.03.

The PEO was obtained from Polysciences Inc. and used as is for all but the contrast matched samples. However, it turns out that a few percent of silica is usually added to PEO in order to improve the flow properties of the powder. This was sufficient to prevent contrast matching of the polymer to the solvent (with an apparent contrast match point for the PEO of 45 vol % D_2O close to that of silica). Moreover, densitometry measurements yielded a PEO density of 1.2 g cm^{-3}. The PEO was thus purified by dissolving 2 wt % of the impure polymer in water and centrifuging the solutions at 3200*g* for 12 h. The supernatant was then removed and freeze-dried. In this way, clean polymer was obtained within 3−4 days. The density of this purified PEO was 0.83 g cm^{-3}, and the match point was found to be the expected 17 vol % D_2O. Samples made from the purified PEO were compared to those made from as-received PEO to verify that the very small amount of silica did not affect any of the microscopic or macroscopic behavior of the system.

Table 2. Characteristic Parameters of PEO Samples Dissolved in Water

molecular weight M_w (kg/mol)	radius of gyration R_g (Å)	hydrodynamic radius R_h (Å)	threshold concentration c^* (w/v, %)
100	177	104	0.72
300	335	194	0.32
600	502	289	0.19
1000	677	387	0.13

Characteristic parameters of aqueous PEO solutions are given in Table 2. These include the PEO molecular weight, M_w, the radius of gyration, R_g, the hydrodynamic radius, R_h, and the overlap threshold concentration, c^*, of each PEO sample dissolved in water at 25 °C. The radius of gyration and the hydrodynamic radius were calculated from the empirical equations suggested by Devanand et al.,[25] who performed dynamic light scattering experiments on aqueous solutions of PEO of different molecular weights.

The solvent used was D_2O, which is generally preferred to H_2O in neutron scattering experiments. Mixtures of D_2O and H_2O were only used for neutron scattering contrast matched experiments. The solvent ratio used to contrast match the laponite clay particles contained 70 vol % D_2O and 30 vol % H_2O. To contrast match the PEO chains, a solvent with 17 vol % D_2O and 83 vol % H_2O was used. To ensure chemical stability of the particles, the pH of the solutions was adjusted to ≈10 by adding NaOH.[26,27] At this pH value, the particles are negatively charged. To screen the electrostatic interactions between the negatively charged particles, the ionic strength of the solutions was adjusted by adding 10^{-3} mol/L NaCl.[26,28] Unfortunately, a decrease of the pH of the samples was observed with time, most probably due to dissolution of CO_2 from the air. Gels whose pH dropped below 8 were discarded. Highly reproducible measurements were possible within a window of 3 months after sample preparation. These samples are abbreviated as LRD*x*-PEO*y*-M_w (in kg/mol), where *x* and *y* denote the weight fraction of laponite and PEO, respectively.

Most of the hydrogels used here were prepared by dissolving the polymer powder first followed by a slow addition of clay powder to the stirring polymer solution. This procedure was first verified to produce similar results to the previously used mixing procedure. That procedure consists of mixing the PEO and the laponite powders together first before adding the solvent. During the initial stages of mixing, large clumps are formed. However, with extensive mixing and centrifuging for a period of 3 weeks, complete dissolution of the polymer and laponite clusters is achieved, and hydrogels that are macroscopically homogeneous and transparent to the eye are obtained.

Small-angle neutron scattering measurements (SANS) were performed at the NIST Center for Neutron Research using both NG3 and NG7 SANS instruments.[29] The typical *q*-range used for these measurements was from 0.0027 to 0.25 Å^{-1}, corresponding to a characteristic distance ($d = 2\pi/q$) probed of ≈2000 to 25 Å. The incident neutron beam had a wavelength of either 6 or 8 Å. Couette cells with gaps of 0.5 and 1 mm were used, giving a total path length through the sample of 1 and 2 mm, respectively. In the standard configuration, referred to as the "radial beam" geometry, the incident beam is parallel to the shear

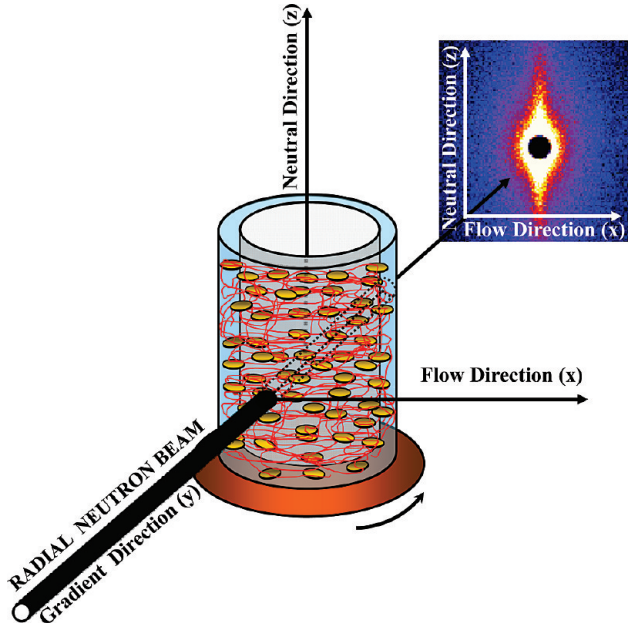

Figure 2. Schematic of a Couette type shear cell illustrating how the radial beam geometry (which is parallel to the shear gradient) passes through the center of the cell and provides information in the flow (x)−neutral (z) plane. When the platelets align under shear with their face normal parallel to the neutral (z) direction, then the radial pattern is anisotropic along the z direction.

gradient. This geometry provides information in the flow (x)−neutral (z) plane (Figure 2). The temperature of the samples was set at 23 °C and was controlled by a thermostatting fluid that circulated around the Couette cell. A solvent trap was used to prevent solvent evaporation. The scattering data from each sample were corrected for background, detector efficiency, empty cell scattering, and sample transmission in the usual way, and intensities were placed on an absolute scale (cm^{-1}) using beam flux measurements.[30]

Ultrasmall-angle neutron scattering (USANS) measurements were also performed at NIST Center for Neutron Research, using the thermal neutron double-crystal diffractometer (BT5).[31] The neutron wavelength was 2.38 Å, and the q-range covered was between 4×10^{-5} and 2.7×10^{-3} $Å^{-1}$. Scattering data were converted to absolute units, cm^{-1}, by subtracting the empty cell scattering and normalizing by the sample thickness. The slit-smeared intensity was numerically desmeared using the SANS-IGOR Pro Software provided by NIST.[30] Only desmeared data are shown here.

In order to characterize the anisotropy in the SANS patterns, annular averages for two different q values were calculated. The annular average gives the intensity, $I_q(\Phi)$, as a function of azimuthal angle, Φ, at a particular $q \pm \Delta q$ (Figure 3), with $\Phi = 0$ being defined as the flow direction. The annular average at $q = 0.0040 \pm 0.0008$ $Å^{-1}$ speaks to the shear responses of large-scale structures (on the order of 150 nm), while the annular average at $q = 0.0100 \pm 0.0008$ $Å^{-1}$ speaks to the shear response of structures on the size scale of individual disks (on the order of 60 nm). Anisotropic objects usually give rise to an isotropic scattering pattern and a flat annular average due to the fact that all orientations are equally probably (and thus equally populated at any given time). However, once anisotropic objects begin to orient preferentially in one direction, the scattering pattern becomes anisotropic which is reflected in the annular average. Further the orientation of different length scales is probed by the q value of the particular annular average. In order to quantify the evolution of the preferential orientations, some measure of the anisotropy is required. A number of different methods have been used, but here we use the Herman's orientation

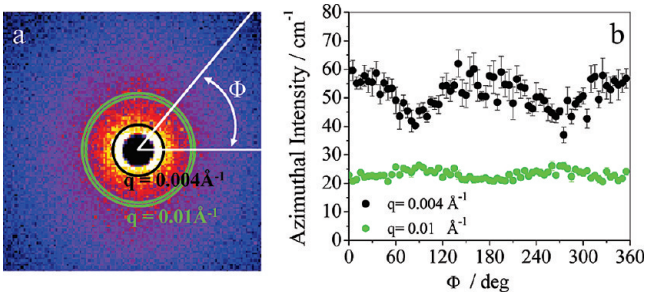

Figure 3. SANS data for the LRD3-PEO2-M_w300 sample at 30 s^{-1}. (a) 2D SANS pattern showing the annular rings of interest at q = 0.004 $Å^{-1}$ and at q = 0.01 $Å^{-1}$. (b) 1D annular average of the intensity from the two q regions of interest plotting $I_q(\Phi)$ as a function of the annular angle Φ (referenced to the flow direction). Anisotropy is clearly visible for the lower q of interest at 0.004 $Å^{-1}$.

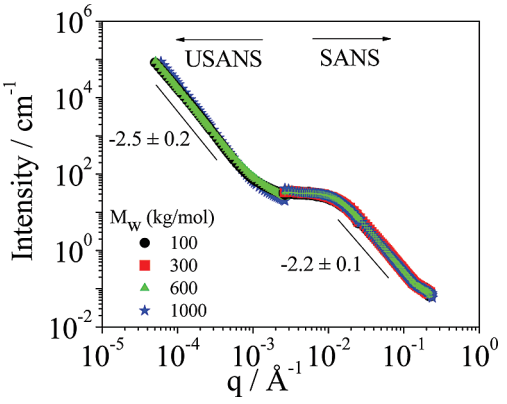

Figure 4. Combined SANS and desmeared-USANS profiles from the LRD3-PEO2-M_w hydrogels at rest. Note: error bars are smaller than the symbols.

function (or Herman parameter) calculated using the following equation:[32,33]

$$f_q = \frac{3\langle \cos^2 \Phi \rangle - 1}{2}$$

where $\langle \cos^2 \Phi \rangle = \dfrac{\int_0^{2\pi} I_q(\Phi) \cos^2 \Phi \sin \Phi \, d\Phi}{\int_0^{2\pi} I_q(\Phi) \sin \Phi \, d\Phi}$

The Herman parameter takes on values from −0.5 to +1.0 with a value of −0.5 indicating complete orientation of the components parallel to the flow direction, a value of +1.0 indicating their complete orientation perpendicular to the flow direction (and parallel to the neutral direction), and a value of 0 indicating completely random orientation of the components.[34]

Results and Discussion

In order to explore the effects of polymer chain length on the structure, gels with a fixed concentration of clay (3 wt % LRD) and polymer (2 wt % PEO) but different molecular weights (M_w) of PEO were prepared (Figure 4). At rest, the network is free of stress, so that the coated-clay particles and the diffuse polymer chains are randomly oriented giving rise to isotropic scattering (Figure 4 and the scattering patterns in the first column of Figure 5). In our previous work[12−16] we presented the SANS data from these systems and suggested that the structure of the network at rest was independent of the molecular weight of the polymer, based on complete overlap of the SANS data for samples with different molecular weight.[12] However, the lowest q of the SANS regime only probes spatial structures at the several platelet size range. By combining data from both SANS and

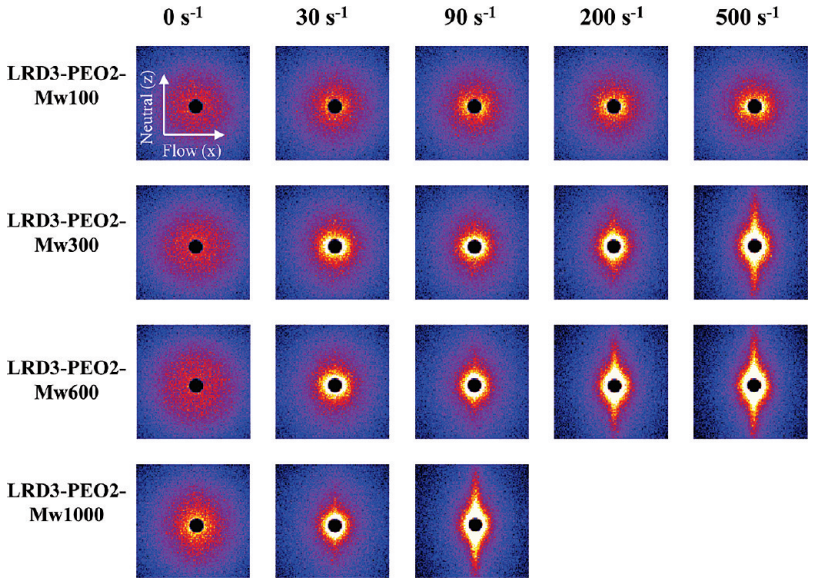

Figure 5. 2D SANS patterns for the four LRD3-PEO2-M_w hydrogels at rest and at different shear rates. The data were collected in the radial geometry with the beam parallel to the shear gradient. High normal forces in the LRD3-PEO2-M_w1000 under shear precluded measurements beyond shear rates of 120 s^{-1}.

USANS scattering profiles covering 4 orders of magnitude in q, from 4×10^{-5} to 0.24 $Å^{-1}$, can be obtained. The fact that at rest the scattering profiles from all the different molecular weight hydrogels overlap at all q indicates that the structures at all length scales, up to tens of micrometers, are indeed completely independent of polymer molecular weight. This is consistent with our hypothesis regarding the structure of the clay network, with the findings of Lal et al.[6,7] and Nelson et al.,[19] showing the adsorbed polymer layer thickness to be independent of molecular weight, and with the fact that the static structure of a polymer network above c^* should also be relatively independent of molecular weight.

The lower q data of the USANS, down to a q of 4×10^{-5} $Å^{-1}$, which probes structures up to several micrometers, exhibit a power law behavior with an exponent of -2.5 ± 0.2, suggesting the existence of a relatively dense network structure up to tens of micrometers length scale. The SEM and TEM data from our work on the samples with M_w = 1000 kg/mol support this view with what appear as clay-rich areas separated by pockets of clay-poor areas.[13] The scattering patterns in the first column of Figure 5 are reminiscent of those seen in pure laponite dispersions[35−39] at concentrations above the sol−gel transition. For example, light scattering experiments by Kroon et al.[35−37] on such pure clay systems yielded a fractal structure with a fractal dimension that evolved from 2.8 to 2.1 during the gelation process. Investigations by Pignon et al.[38,39] also suggested the existence of a network structure with a fractal dimension of 3 up to length scales of a few micrometers, followed by a more open structure with a fractal dimension of 1.8.

The high q data in the SANS regime (Figure 4) cannot be fit with the form factor of a disk (or coated disk), and the slope of −2.2 deviates slightly from the −2 slope of a disklike structure indicating a non-negligible contribution from the free polymer. While the dense clay is expected to contribute most strongly to the scattering compared to the typically loose structure of polymer networks, the polymer scattering will not be zero. This was confirmed by data obtained from an LRD3-PEO2-M_w600 where the polymer was contrast matched to the solvent, rendering it invisible and leading to the scattering arising solely from the clay particles (Figure 6). In this case the high q data have the expected −2 slope though no quantitative fits are possible due to the

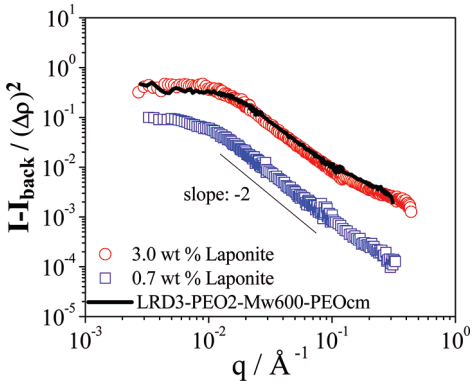

Figure 6. Scattering intensity normalized by contrast showing the superposition of scattering data from a pure 3 wt % laponite dispersion and from a 3 wt % laponite in a solution of 2 wt % PEO (M_w = 600 kg/mol) with the PEO contrast matched to the solvent (LRD3-PEO2-M_w600PEOcm). The dilute 0.7 wt % laponite data from Figure 1 is also plotted.

interactions evident at these concentrations and the fact that no models currently exist to describe the structure factor for highly anisotropic particles. To explore this further, a solution of 3 wt % laponite in D_2O was measured. After correction for the relative contrast terms, the PEO contrast matched data superimpose nicely on the data for pure laponite (Figure 6). Finally, since the shape (form factor) for the clay particle is independent of concentration, the data for 3 wt % laponite can be divided by the form factor derived from the fit to the dilute 0.7 wt % solution described in the Experimental Section to yield the structure factor shown in Figure 7. The first oscillation is clearly visible with the primary peak at 0.019 ± 0.002 $Å^{-1}$ indicating a nearest-neighbor spacing of roughly 33 nm.

Despite the low signal and high background inherent in polymer contrast matched measurements, it is clear that, as expected, the structure of the laponite in the polymer−clay system is unperturbed from that in the pure laponite system, up to length scales of several particles. This, coupled with the similarity of the scattering profiles with those of pure laponite from the literature over the entire q range, leads us to speculate that the basic structure of the laponite gel may not be significantly

perturbed by the addition of polymer. This is consistent with the most recent conclusions of Bruyn et al.[5] using a different laponite clay. Unfortunately, we were unable to measure the PEOcm LRD3-PEO2-M_w in the USANS regime necessary to unambiguously demonstrate this hypothesis in these systems.

As a shear deformation is applied, however, the effect of the polymer−clay interactions becomes apparent as the patterns begin to exhibit anisotropic characteristics (Figure 5). At the very lowest shear rates, the scattering patterns are characterized by an increase of the very low q intensity in the direction parallel to the flow field (x direction), often referred to in the literature as "butterfly patterns". At higher shear rates, and extending out to high q, an anisotropic scattering pattern (vertical streak) develops in the neutral (z) direction, but only for the higher molecular weight samples. The shear-SANS results are summarized in Figure 8 by plotting the Herman parameter at both q values (0.01 and 0.004 Å^{-1}) as a function of shear rate for each of the gels in the series (LRD3-PEO2-M_w100, 300, 600, 1000).

At the high q of 0.01 Å^{-1} (probing the smaller length scales), the LRD3-PEO2-M_w100 sample behaves very similarly to a pure 3 wt % laponite gel with the Herman parameter fluctuating around zero indicating no obvious orientation of objects on these length scales to the highest shear rates accessible. However, the samples containing larger molecular weight PEO, LRD3-PEO2-M_w300, 600, and 1000 all display increasingly negative values of the Herman parameter with increasing shear rate consistent with our previous more qualitative results, indicating that under bridging conditions the clay disks align in the flow field with their surface normal parallel to the neutral direction.[12−16] This effect is more pronounced as the polymer molecular weight increases consistent with an increased network strength by, for example, bridging second nearest neighbors or by tethering more than two clay particles.

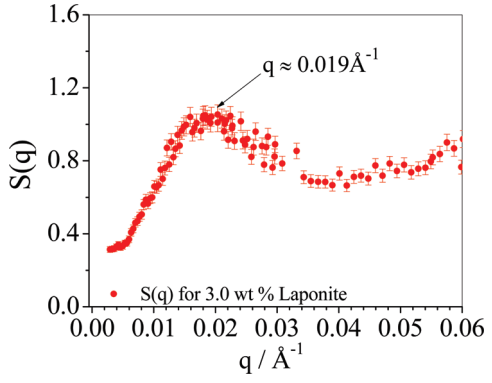

Figure 7. Structure factor, $S(q)$, for a 3 wt % pure laponite dispersion, showing a peak at 0.019 ± 0.002 Å^{-1} indicating a nearest-neighbor spacing of roughly 33 nm.

Interestingly, at the lower q of 0.004 Å^{-1} all the hydrogels exhibit anisotropic scattering patterns with positive values of the Herman parameters at low shear rates, indicating the existence of the so-called butterfly pattern for all samples studied. For the polymer molecular weight samples above which our previous work suggested bridging begins to occur (all except the sample with M_w = 100 kg/mol), the value of this low q Herman parameter begins to decrease at higher shear rates and then changes sign, indicating a different orientation at high shear. The range of shear rates at which butterfly patterns are observed is different for each sample, decreasing and shifting to lower values with increasing polymer molecular weight. For the lowest polymer molecular weight sample (M_w = 100 kg/mol), on the other hand, where no bridging is expected, the Herman parameter at this low q remains positive and continues to increase slightly to the highest shear probed.

The very low q nature of the butterfly suggests that some relatively large elongated structures are orienting along the neutral direction at even the lowest shears. The fact that the butterfly occurs for both the "bridged" and "not bridged" samples indicates however that it is independent of any bridging interactions. Oriented large-scale structures induced by flow and exhibiting butterfly patterns have been observed in a variety of systems such as short chain polymer swollen networks,[40] clay suspensions,[41] entangled polymer melts,[42] wormlike micelles,[43,44] and many more.[45−48] Vermant[49] points out that large-scale structures can develop under shear in weakly attractive colloidal systems that form intrinsically inhomogeneous dispersions. While our system is clearly more complex than a simple weakly interacting system, the USANS data (Figure 4) and previously published ESEM images[13] demonstrate the large-scale sponge-like structures that exist at rest in these polymer−clay gels. It would appear then that the large-scale sponge may break up into domains which, given the shear gradient perpendicular to the flow, may in turn roll up around the neutral axis, thus leading to the elongation of the structures in that direction (or more precisely shrinking of the other two dimensions).

The reversal of sign of the low q Herman parameter could naively be interpreted as a reversal of orientation at high shear in the systems where the polymer bridges the clay particles. However, the higher q Herman parameter remains zero for all samples at the lower shear rates and becomes negative at higher shears only for those in which bridging is thought to be significant, exactly where the lower q Herman parameter begins to reverse. Further, the q value probed by this Herman parameter is well within the plateau region of Figure 4 which includes contributions from the platelet interaction peak and the tail of the large-scale structure scattering along with the disk form factor. Thus, another, perhaps more likely interpretation would be that at high shear the signal from the platelet orientation begins to dominate the scattering, masking out the signal from any oriented large-scale structure. In order to qualitatively verify this hypothesis,

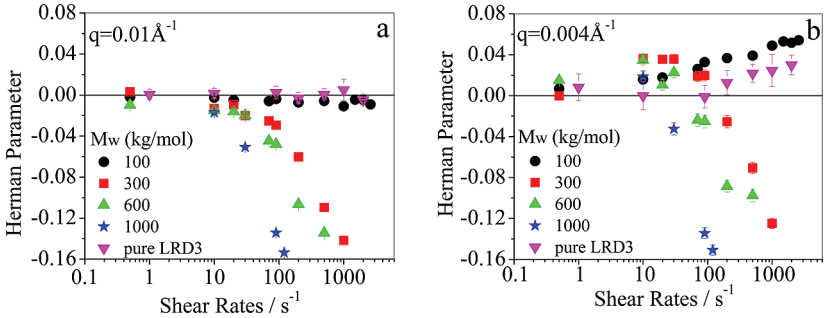

Figure 8. Herman parameter calculated at q values of 0.01 Å^{-1} (a) and 0.004 Å^{-1} (b) as a function of shear rate for the different molecular weight hydrogels. For comparison, data from a pure 3 wt % laponite solution are also plotted.

small-angle light scattering (SALS), which probes much lower q values in 2D, was performed on all these systems (Figure 9 shows some representative patterns). In each case a clear butterfly is visible at all shear rates used here. Further, Gibson et al.[17,18] observed similar SALS "butterfly" patterns at high shear for the very highest molecular weight sample used of 1000 kg/mol for the same composition. These authors attributed the emergence of those patterns to transient micrometer-scale heterogeneities that develop under shear. Thus, it is clear that the large-scale structure and its orientation under flow are completely independent of bridging.

In previous work, the fact that no nanoscale alignment occurs in the lowest polymer molecular weight sample (the sample with M_w = 100 kg/mol) was cited as support for the idea that the platelet orientation under flow is due to the polymer bridging clay platelets.[12−15] However, given that the degree of orientation decreases with polymer molecular weight, the amount of polymer available after coating the clay strongly depends on the available clay surface, the clay surface area in turn strongly depends on the exact size distribution, and the polymer overlap concentration decreases with polymer molecular weight in the same way the Herman parameter does, the question arises as to whether a significant portion of the effect may come simply from the polymer network structure that occurs above the overlap concentration, c^*, rather than from individual polymer strands bridging clay platelets. In order to more thoroughly test the bridging hypothesis, measurements were made that vary both the polymer and clay concentrations. Figures 10 and 11a,b show the Herman parameter (for both q values of 0.01 and 0.004 Å^{-1}) as a function of shear rate, for a fixed 3 wt % LRD clay concentration. In Figure 10, the polymer concentration of lowest molecular weight polymer of 100 kg/mol, where the polymer concentration may have dropped slightly below c^*, is increased while in Figure 11a,b the concentration of the 300 kg/mol polymer, which may be just above c^*, is decreased. The extent of the concentration variations was limited by the phase diagram of the systems. Nonetheless, the results provide a striking confirmation of the hypothesis.

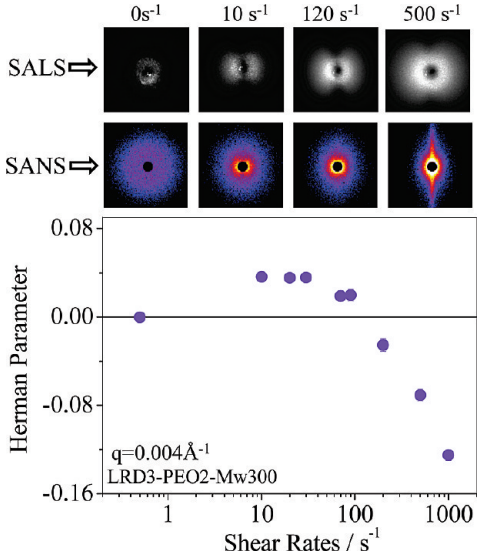

Figure 9. Herman parameter calculated for the LRD3-PEO2-M_w300 sample at the lower q value of 0.004 Å^{-1}. 2D shear-SALS and shear-SANS patterns are shown above the plot.

The complete lack of any significant change in the shear response of the sample with M_w = 100 kg/mol despite an increase in the polymer concentration by a factor of 2.5 clearly demonstrates that the semidilute nature of the polymer solution is not a contributor in this case. The effects however of decreasing the concentration in the sample with M_w = 300 kg/mol is more surprising with the strength of the high q Herman parameter (Figure 11a) increasing significantly with decreasing polymer concentration while the low q butterfly pattern (Figure 11b) of the large-scale structures oriented along the neutral direction (positive Herman parameter) remains visible to much higher shear rates before any signature of orientation in the flow direction develops (negative Herman parameter). The fact that the effect does not decrease with decreasing concentration is further very strong evidence that it does not arise from the existence of an entangled polymer network in the semidilute regime. However, a more detailed explanation of the bridging mechanism is required to completely understand the observed phenomenon.

As long as neither the clay concentration (average center-to-center distance of the clay particles) nor the polymer molecular weight (length of each individual polymer strand) changes, one might expect the effect to remain relatively constant with decreasing polymer concentration until one approaches the concentration required to simply coat the clay, at which point the effect should disappear rather rapidly with concentration. However, given the clay surface is always coated with polymer in an absorption−desorption equilibrium, all the EO segments must increasingly compete for that limited surface area once the polymer concentration exceeds what is required for complete coverage. Thus, as the concentration increases, the chances of a given polymer successfully competing for surface area simultaneously on two adjacent platelets (causing bridging) must in fact decrease, leading to the observed decrease in orientation. In this case, lowering the clay concentration at a fixed polymer concentration and molecular weight should diminish the orientation effect for two reasons: the increasing interparticle distance for a fixed bridging polymer size and an increasing competition for the decreasing surface area. Figure 11c,d shows results for a fixed

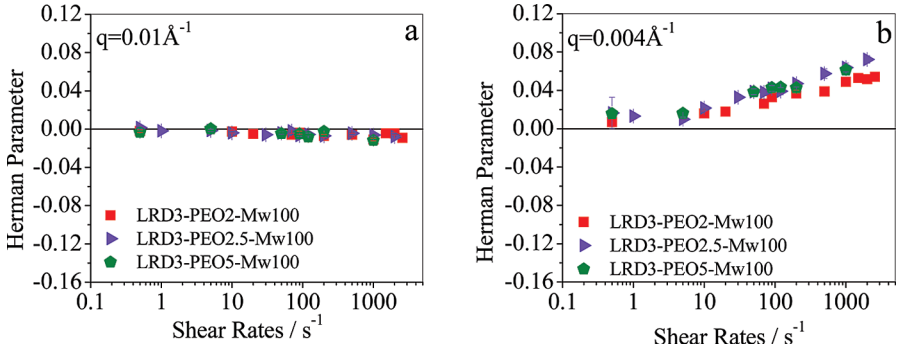

Figure 10. Polymer concentration dependence of the Herman parameter calculated at q values of 0.01 Å^{-1} (a) and 0.004 Å^{-1} (b) as a function of shear rate for the LRD3-PEOy-M_w100 samples.

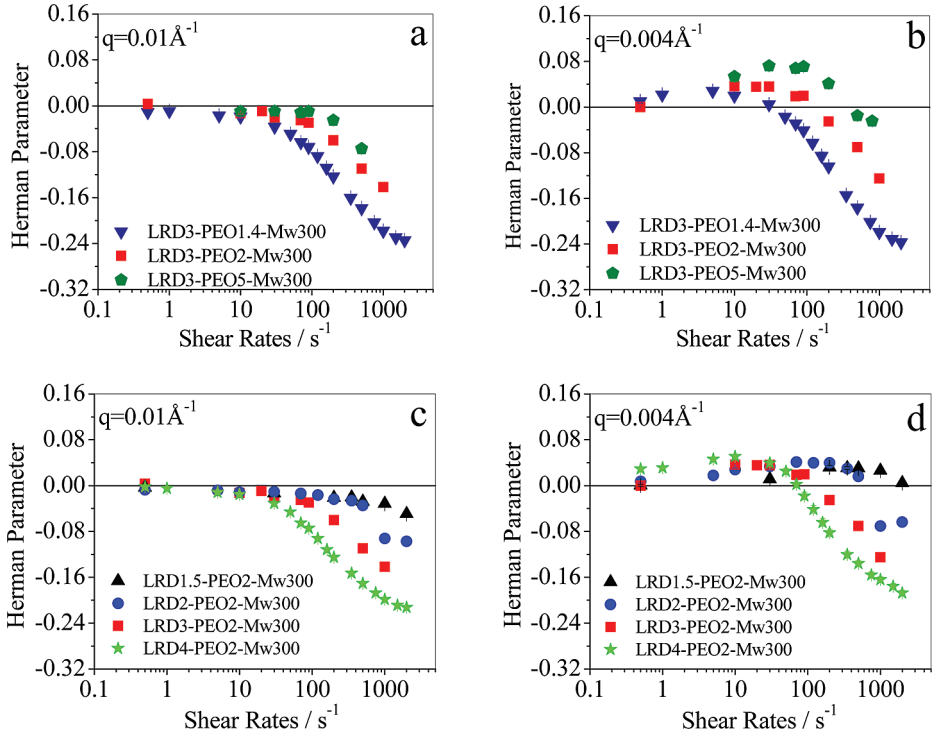

Figure 11. Herman parameter as a function of shear rate for the LRDx-PEOy-M_w300 samples: (a, c) calculated at $q = 0.01$ Å^{-1}; (b, d) calculated at $q = 0.004$ Å^{-1}; (a, b) varying polymer concentration at a fixed clay concentration; (c, d) varying clay concentration at a fixed polymer concentration.

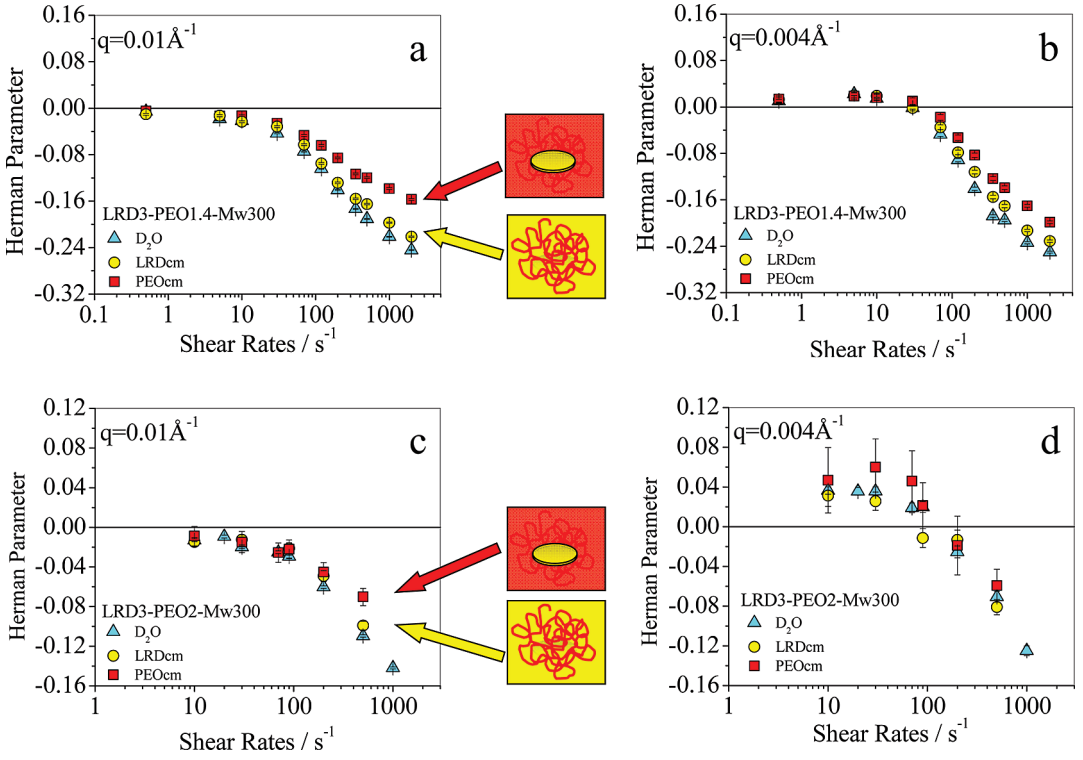

Figure 12. Herman parameter as a function of shear rate for both D_2O dispersions and dispersion in contrast matched solvents: (a, c) calculated at $q = 0.01$ Å^{-1}; (b, d) calculated at $q = 0.004$ Å^{-1}; (a, b) calculated for the LRD3-PEO1.4-M_w300 sample; (c, d) calculated for the LRD3-PEO2-M_w300 sample.

polymer concentration of 2 wt % PEO with a varying clay concentration. As expected, the nanoscale orientation (at $q = 0.01$ Å^{-1}) (Figure 11c) becomes weaker while the butterfly pattern (at $q = 0.004$ Å^{-1}) remains visible to higher shear rates (Figure 11d), with decreasing clay concentration.

This then suggests that in fact there is a "sweet spot" at a concentration just slightly above that required for complete coverage where the bridging effect would be a maximum. It is interesting to note (Figure 11b,d) that at a fixed clay concentration the increasing polymer concentration (or at a fixed polymer

concentration the decreasing clay concentration) which decreases the bridging also dramatically increases the strength of the butterfly and the shear rate to which it is visible, in further strong support of the previously mentioned hypothesis regarding the apparent "reversal" of the large-scale structural orientation seen at low q. The higher the bridging density, the stronger the clay orientation, leading to a quicker overwhelming of the oriented large-scale structure signal (butterfly pattern).

Finally, a better understanding of the alignment process itself requires an understanding of how the individual components react to the applied shear. To this end two systems were studied: the base system of LRD3-PEO2-M_w300 (Figure 12c,d) and the LRD3-PEO1.4-M_w300 (Figure 12a,b) just shown to exhibit even stronger nanoscopic alignment. For both systems, two H_2O/D_2O solvent mixtures were used such that the scattering length density of the solvent was matched to either the PEO (abbreviated as PEOcm) where the scattering arises only from the clay in the presence of (the now invisible) polymer or the laponite particles (abbreviated LRDcm) with the scattering coming only from the polymer with the clay platelets still contributing to the macroscopic properties of the sample but completely invisible to the neutrons. The Herman parameter (at both q values of 0.004 and 0.01 $Å^{-1}$) is given in Figure 12. The occurrence of the butterfly pattern under all contrast conditions clearly reveals that both polymer and clay contribute to these oriented large-scale structures. While expected from the hypothesis derived from USANS and electron microscopy results, it does preclude the alternate possibility that the oriented structure could be an induced structure forming from the free polymer in solution.

Analysis of the high q (q = 0.01 $Å^{-1}$) Herman parameter, particularly for the lower polymer concentration where the bridging effect is maximum and the signal is therefore the strongest, shows that at low shears the polymer and clay align to the same extent. However, as the shear increases, the polymer (clay contrast matched) begins to align more strongly than the clay. Understanding the polymer orientation data is complicated by the fact that there are three different polymer components. First is the polymer coating the clay whose alignment must mirror that of the clay. Second is the polymer bridging one or more clay platelets, and finally is the free polymer in solution. Given that a system of polymer alone will not align, one can assume that the free polymer does not contribute to the orientation. Of the remaining components, the coating polymer clearly cannot orient more than the clay it is coating. This leads to the conclusion that at high shears the bridging polymer must be significantly stretched such that its alignment factor is stronger than for the clay. This supports the suggestion of Schmidt et al.,[15] who studied an LRD3-PEO2-M_w1000 sample using shear-SANS and flow-birefringence, that the clay platelets align first, followed by a stretching of the interconnected polymer chains.

Conclusions

The structural properties of these hydrogels at rest appear to be dominated by the clay structure which is relatively weakly perturbed by the addition of polymer. It is only under deformation that the polymer's contribution becomes evident, significantly affecting the dynamical response of the system. As long as the polymer molecular weight is below that required to easily bridge neighboring clay platelets at the given clay concentration, no alignment of clay platelets or polymer occurs. However, above that molecular weight, the clay platelets align under the influence of shear in the unexpected "a-orientation" with the platelet normal parallel to the neutral direction. Eventually the polymer strands themselves appear to align in the direction of the flow. Aside from having a size sufficient to bridge neighboring platelets, the concentration of polymer relative to that of the clay is an important factor. Indeed, as the polymer concentration increases relative to the clay concentration, the PEO segment competition for available clay surface area increases, thus decreasing the chances for a single polymer to connect simultaneously more than one platelet in the constant absorption/desorption equilibrium. This suggests a maximum bridging effect slightly above the concentration required for full coating of the clay. The large-scale structural alignment, on the other hand, while clearly incorporating both the polymer and the clay, is completely independent of any effective cross-linking of the clay by the polymer. This alignment is no doubt due to a "rolling up" of the fractal-like network which contributes to the shear thinning of these systems that is hampered by the interconnectivity of the bridging network.

The implications for materials design are clear: the clay concentration determines most of the static properties, while the dynamic responses are tuned by adjusting the polymer molecular weight with respect to the chosen clay concentration and choosing a polymer concentration for the strength of connectivity desired, where a maximum bridging effect would be slightly above what is required for complete coverage. Other parameters such as clay or polymer polydispersity, clay aspect ratios, salt concentration, types of salt, and pH would clearly complicate the simple picture but provide many more "knobs" for tuning the material. Further study will be required to elucidate those effects.

Acknowledgment. This research has been supported by the National Institute of Standards and Technology, NIST awards 60NANB6D6159 and 60NANB6D6096, and in part by an NSF CAREER award to G.S. We acknowledge the support of the National Institute of Standards and Technology, U.S. Department of Commerce, in providing the neutron research facilities used in this work. This work utilized facilities supported in part by the National Science Foundation under Agreement DMR-0454672. The authors thank Professor D. Pozzo of the University of Washington for providing the flow SALS images. Certain commercial materials and suppliers are identified in this paper to foster understanding. Such identification does not imply recommendation or endorsement by the National Institute of Standards and Technology, nor does it imply that the materials or equipment identified are necessarily the best available for the purpose.

References and Notes

(1) Ohno, K.; Koh, K.; Tsujii, Y.; Fukuda, T. *Macromolecules* **2002**, *35*, 8989–8993.
(2) Merkel, T. C.; Freeman, B. D.; Spontak, R. J.; He, Z.; Pinnau, I.; Meakin, P.; Hill, A. J. *Science* **2002**, *296* (5567), 519–522.
(3) Shibayama, M.; Suda, J.; Karino, T.; Okabe, S.; Takehisa, T.; Haraguchi, K. *Macromolecules* **2004**, *37* (25), 9606–9612.
(4) Shibayama, M.; Karino, T.; Miyazaki, S.; Okabe, S.; Takehisa, T.; Haraguchi, K. *Macromolecules* **2005**, *38* (26), 10772–10781.
(5) de Bruyn, J. R.; Pignon, F.; Tsabet, E.; Magnin, A. *Rheol. Acta* **2008**, *47* (1), 63–73.
(6) Lal, J.; Auvray, L. *J. Appl. Crystallogr.* **2000**, *33* (1), 673–676.
(7) Lal, J.; Auvray, L. *Mol. Cryst. Liq. Cryst.* **2001**, *356*, 503–515.
(8) Baghdadi, H. A.; Sardinha, H.; Bhatia, S. R. *J. Polym. Sci., Part B: Polym. Phys.* **2005**, *43* (2), 233–240.
(9) Pozzo, D. C.; Walker, L. M. *Colloids Surf., A* **2004**, *240* (1−3), 187–198.
(10) Zebrowski, J.; Prasad, V.; Zhang, W.; Walker, L. M.; Weitz, D. A. *Colloids Surf., A* **2003**, *213* (2−3), 189–197.
(11) Can, V.; Okay, O. *Des. Monomers Polym.* **2005**, *8* (5), 453–462.
(12) Loizou, E.; Butler, P. D.; Porcar, L.; Schmidt, G. *Macromolecules* **2006**, *39* (4), 1614–1619.
(13) Loizou, E.; Butler, P. D.; Porcar, L.; Talmon, Y.; Kesselman, E.; Schmidt, G. *Macromolecules* **2005**, *38*, 2047–2049.
(14) Schmidt, G.; Nakatani, A. I.; Butler, P. D.; Han, C. C. *Macromolecules* **2002**, *35* (12), 4725–4732.
(15) Schmidt, G.; Nakatani, A. I.; Butler, P. D.; Karim, A.; Han, C. C. *Macromolecules* **2000**, *33* (20), 7219–7222.

(16) Schmidt, G.; Nakatani, A. I.; Han, C. C. *Rheol. Acta* **2002**, *41* (1−2), 45–54.
(17) Lin-Gibson, S.; Kim, H.; Schmidt, G.; Han, C. C.; Hobbie, E. K. *J. Colloid Interface Sci.* **2004**, *274* (2), 515–525.
(18) Lin-Gibson, S.; Schmidt, G.; Kim, H.; Han, C. C.; Hobbie, E. K. *J. Chem. Phys.* **2003**, *119* (15), 8080–8083.
(19) Nelson, A.; Cosgrove, T. *Langmuir* **2004**, *20* (6), 2298–2304.
(20) Nelson, A.; Cosgrove, T. *Langmuir* **2004**, *20* (24), 10382–10388.
(21) Schexnailder, P.; Loizou, E.; Porcar, L.; Butler, P.; Schmidt, G. *Phys. Chem. Chem. Phys.* **2009**, *11* (15), 2760–2766.
(22) Daga, V. K.; Wagner, N. J. *Rheol. Acta* **2006**, *45* (6), 813–824.
(23) Malwitz, M. M.; Butler, P. D.; Porcar, L.; Angelette, D. P.; Schmidt, G. *J. Polym. Sci., Part B: Polym. Phys.* **2004**, *42* (17), 3102–3112.
(24) www.scprod.com/pdfs/LaponiteBrochureE.pdf.
(25) Devanand, K.; Selser, J. C. *Macromolecules* **1991**, *24*, 5943–5947.
(26) Tanaka, H.; Meunier, J.; Bonn, D. *Phys. Rev. E* **2004**, *69*, 031404.
(27) Thompson, D. W.; Butterworth, J. T. *J. Colloid Interface Sci.* **1992**, *151* (1), 236–243.
(28) Levitz, P.; Lecolier, E.; Mourchid, A.; Delville, A.; Lyonnard, S. *Europhys. Lett.* **2000**, *49* (5), 672–677.
(29) Glinka, C. J.; Barker, J. G.; Hammouda, B.; Krueger, S.; Moyer, J. J.; Orts, W. J. *J. Appl. Crystallogr.* **1998**, *31*, 430–445.
(30) Kline, S. R. *J. Appl. Crystallogr.* **2006**, *39*, 895–900.
(31) Barker, J. G.; Glinka, C. J.; Moyer, J. J.; Kim, M. H.; Drews, A. R.; Agamalian, M. *J. Appl. Crystallogr.* **2005**, *38*, 1004–1011.
(32) Somani, R. H.; Yang, L.; Hsiao, B. S.; Sun, T.; Pogodina, N. V.; Lustiger, A. *Macromolecules* **2005**, *38* (4), 1244–1255.
(33) Roe, R. J. *Methods of X-Ray and Neutron Scattering in Polymer Science*; Oxford University Press: New York, 2000.
(34) In principle, as a single value, the Herman parameter is a measure of both the angle of the center of the orientational distribution, relative to the flow direction, as well as the width of that distribution. However, in our case all distributions are centered either at 0° or at 90° so that it can be used as a measure of the width of the distribution.
(35) Kroon, M.; Vos, W. L.; Wegdam, G. H. *Phys. Rev. E* **1998**, *57* (2), 1962–1970.
(36) Kroon, M.; Vos, W. L.; Wegdam, G. H. *Int. J. Thermophys.* **1998**, *19* (3), 887–894.
(37) Kroon, M.; Wegdam, G. H.; Sprik, R. *Phys. Rev. E* **1996**, *54* (6), 6541–6550.
(38) Pignon, F.; Magnin, A.; Piau, J. M.; Cabane, B.; Lindner, P.; Diat, O. *Phys. Rev. E* **1997**, *56* (3), 3281–3289.
(39) Pignon, F.; Piau, J. M.; Magnin, A. *Phys. Rev. Lett.* **1996**, *76* (25), 4857–4860.
(40) Ramzi, A.; Zielinski, F.; Bastide, J.; Boue, F. *Macromolecules* **1995**, *28* (10), 3570–3587.
(41) Pignon, F.; Magnin, A.; Piau, J. M. *Phys. Rev. Lett.* **1997**, *79* (23), 4689–4692.
(42) Hayes, C.; Bokobza, L.; Boue, F.; Mendes, E.; Monnerie, L. *Macromolecules* **1996**, *29* (14), 5036–5041.
(43) Wheeler, E. K.; Izu, P.; Fuller, G. G. *Rheol. Acta* **1996**, *35* (2), 139–149.
(44) Kadoma, I. A.; vanEgmond, J. W. *Phys. Rev. Lett.* **1996**, *76* (23), 4432–4435.
(45) Mendes, E.; Oeser, R.; Hayes, C.; Boue, F.; Bastide, J. *Macromolecules* **1996**, *29* (17), 5574–5584.
(46) Bastide, J.; Leibler, L. *Macromolecules* **1988**, *21* (8), 2647–2649.
(47) Belzung, B.; Lequeux, F.; Vermant, J.; Mewis, J. *J. Colloid Interface Sci.* **2000**, *224* (1), 179–187.
(48) Degroot, J. V.; Macosko, C. W.; Kume, T.; Hashimoto, T. *J. Colloid Interface Sci.* **1994**, *166* (2), 404–413.
(49) Vermant, J. *Curr. Opin. Colloid Interface Sci.* **2001**, *6* (5−6), 489–495.